www.sciencemag.org/content/357/6349/378/suppl/DC1

Supplementary Materials for

Tough adhesives for diverse wet surfaces

J. Li, A. D. Celiz,* J. Yang,* Q. Yang, I. Wamala, W. Whyte, B. R. Seo, N. V. Vasilyev, J. J. Vlassak, Z. Suo, D. J. Mooney†

*These authors contributed equally to this work.
†Corresponding author. Email: mooneyd@seas.harvard.edu

Published 28 July 2017, *Science* **357**, 378 (2017)
DOI: 10.1126/science.aah6362

This PDF file includes:

Other Supplementary Material for this manuscript includes the following:
(available at www.sciencemag.org/content/357/6349/378/suppl/DC1)

Materials and Methods

Materials

High molecular weight sodium alginate (M_W = 265kDa) with high guluronate content (LF20/40; PROTANAL FMC Technologies) was used for in vitro experiments. Low molecular weight sodium alginate (5Mrad) was prepared by irradiating the high molecular weight sodium alginate (LF20/40; PROTANAL FMC Technologies) under γ-rays at a dose of 5 Mrad following the previous protocol (*31*). Ultrapure sodium alginate with low endotoxin levels (MVG and VLVG; ProNova Biomedical AS) was used for in vivo studies. Chitosan of low-, medium- and high-molecular weight was purchased from Sigma and used for in vitro experiments, and ultrapure chitosan (CL214; FMC Corporation) with low endotoxin levels was used for in vivo experiments. The bridging polymers including polyallylamine, gelatin, and polyethyleneimine were purchased from Sigma, and type I collagen was purchased from Advanced BioMatrix. The coupling reagents, 1-ethyl-3-(3-dimethylaminopropyl) carbodiimide hydrochloride (EDC) and N-hydroxysulfosuccinimide (sulfo-NHS), were purchased from Thermo Fisher Scientific. Medical grade cyanoacrylate (Loctite 4541 Prism) was purchased from Henkel Corporation. Monomers including acrylamide (AAm), *N*,*N'*-methylenebis(acrylamide) (MBAA), hydroxyethyl methacrylate (HEMA), free-radical initiator ammonium persulfate (APS), photoinitiator IRGACURE 2959 (I2959) and polymerization accelerator tetramethyl-ethylenediamine (TEMED) were purchased from Sigma. Polyethylene glycol diacrylate (PEGDA) was synthesized following a modified protocol (*32*). Fluorescein isothiocyanate-labeled chitosan (FITC-chitosan) was synthesized according to the previously reported protocol (*33*). Fluorescent microspheres of 500nm diameter with surface carboxylate groups were purchased from Thermo Fisher Scientific. COSEAL surgical sealant and SURGIFLO hemostatic matrix were obtained from Baxter and Ethicon, respectively. Porcine skin, liver, heart, lung and cartilage were purchased from a local grocery store.

Methods

Synthesis of Tough adhesive. To prepare a tough adhesive (TA) in the form of a preformed patch, a hydrogel was first fabricated to provide the dissipative matrix, and then its surface was treated with the bridging polymer and coupling agents for carbodiimide coupling reaction. Alginate-polyacrylamide hydrogels were synthesized following a modified protocol based on a previously reported protocol (*34*). In brief, sodium alginate (LF20/40 and 5Mrad at 1:1 ratio) and acrylamide were first dissolved in HBSS at 2% and 12% respectively, and stirred overnight till a clean solution was obtained. This solution of 10mL was then mixed with 36μL of 2% covalent cross-linker MBAA, 8μL of accelerator TEMED, 226μL of 0.27M initiator APS, and 191μL of 0.75M ionic cross-linker $CaSO_4$ slurries. The mixture was gelled inside a closed glass mold at room temperature overnight.

The bridging polymers polyallylamine, chitosan, gelatin, and polyethyleneimine were dissolved into MES buffer at 2.0% and the pH was adjusted to 6. The collagen was used as a stock solution (1.0%). 1-ethyl-3-(3-dimethylaminopropyl) carbodiimide (EDC), sulfated or unsulfated N-hydroxysuccinimide (NHS) were used as the coupling reagents. The final concentrations of EDC and NHS in the solution of the bridging polymer were both 12mg/mL. The mixture of the bridging polymer and coupling reagents (~250 μL) was applied to the surface of the dissipative matrix (15x70 mm^2) prior to application. Compression was applied before mechanical testing, typically for 5-30 minutes unless stated otherwise. During the waiting time, the specimens were sealed in plastic bags to prevent water loss.

Adhesion Energy Measurement. The adhesion performance was quantified as the adhesion energy, namely the amount of energy required to increase a unit area of interfacial crack. The adhesion energy was determined with either peeling adhesion tests, or bilayer adhesion tests when the substrate had low bulk toughness.

Peeling Adhesion Test. The adhesion energy was measured with 180 degree peeling tests. A ribbon of the tough adhesive (15x1.5x80 mm^3) was adhered to a substrate with one end open, forming a bilayer with an edge crack. The back of TA was also bonded to a rigid polyethylene terephthalate (PET) film with Krazy Glue, in order to limit deformation to the crack tip, and thus all the work done by the machine would be equal to the energy dissipated at the crack tip. The free ends of TA and the substrate were attached to plastic sheets, to which the machine grips were attached. An Instron machine (model 3342 with load cell of maximum 50N) was used to apply unidirectional tension, while recording the force and the extension. The loading rate was kept constant at 100 mm/min. The adhesion energy was two times the plateau value of the ratio of the force and width (*35*).

Bilayer Adhesion Test. When hydrogels of low bulk toughness were tested, a bilayer adhesion test was used to measure adhesion energy (*36*). The hydrogels tested with this method include polyacrylamide, poly(hydroxyethyl methacrylate) and poly(N'-isopropylacrylamide) hydrogels. The bilayer specimens were prepared by compressing TA of 45x20x1.5 mm^3 on a hydrogel of 30x20x1.5 mm^3. A notch was introduced at length 5mm. A rigid polyethylene terephthalate (PET) film with thickness 120 μm (Transparency Copy Film, PP2500, 3M) was glued to the testing hydrogel as a backing layer with Krazy glue. The specimen was stretched by an Instron machine with a constant loading rate of 0.5mm/s, while the force-stretch curves were recorded. The adhesion energy G can be calculated by $G = P(\lambda - 1) - U_s(\lambda)$, where P and λ are the critical force per unit width (the force in the current state divided by the width of the sample in the un-deformed state) and the critical stretch when debonding occurs (*36*). U_s is the strain energy stored in the substrate divided by the area of the substrate in the undeformed state when debonding occurs, which is the area under the recorded force-stretch curve of the

substrate with stretch from 1 to λ. In the case that both arms were glued to the PET film, the adhesion energy $G = P(\lambda - 1)$.

Penetration of Bridging Polymer. Interpenetration of the bridging polymer into the dissipative matrix of TA was imaged using FITC labeled chitosan and confocal microscopy. The FITC-chitosan was dissolved into MES buffer to 2 wt% with pH adjusted to 6, and then 20 μL was distributed on the surface of a hydrogel disk of diameter 6 mm with or without EDC/NHS. The incubation time was varied from 2 to 30 minutes, before aspirating the excess FITC-chitosan solution. Fluorescent microspheres of 20 μL volume were added onto the same hydrogel surface, followed by extensive rinsing with PBS for 30 seconds. The fluorescent microspheres carry carboxylate groups on their surface that can bind with the primary amines on the FITC-chitosan, forming amide bonds via carbodiimide chemistry. A confocal fluorescence microscopy (Zeiss LSM710) was used to image the gel surface, with the excitation wavelengths set to 490 nm for FITC and 588 nm for the fluorescent microspheres.

Confocal Imaging of Adhesion Interface. TA was prepared using FITC-chitosan as the bridging polymer, and adhered to porcine skin, muscle or polyacrylamide hydrogels. Adhesion was performed in the dark, and allowed to develop for one hour. The samples were cryoprotected in 20% sucrose/PBS at room temperature and embedded in OCT before being frozen on dry ice. Transverse cryosections (50 μm) were cut using a cryostat (Leica CM1950) and imaged by confocal fluorescence microscopy (Zeiss LSM710). The excitation wavelength of FITC was set to be 490 nm, and bright field images were also collected.

Matrix Toughness Measurement. Pure shear tests were carried out to measure the matrix toughness. In brief, rectangular specimens (50x5x1.5 mm^3) were stretched by an Instron machine (model 3342 with load cell of maximum 1000N). For notched samples, an edge crack of length 20mm was cut using a razor blade in the middle of the gauge section of the specimen. The stretch rate was fixed at 2 min^{-1}. From the stress-stretch curves of the unnotched and notched specimens, the matrix toughness was calculated following the method reported previously (*34*).

Effects of Concentration and Molecular Weight of Chitosan on Adhesion. This study investigated how the adhesion depended on the concentration and molecular weight of the bridging polymer. The chitosan concentration was varied from 0.3 to 1.5 wt% in preparing TA. The molecular weight of the chitosan was varied by using low, medium and high molecular-weight chitosan purchased from Sigma. The resulting adhesives were applied onto an alginate-polyacrylamide hydrogel as a model substrate, and the adhesion energy was measured with peeling adhesion tests.

Sterile Processing. Endotoxin-free alginate (MVG and VLVG) and chitosan (CL214) were used in the in vitro cell culture and in vivo animal studies. The alginate and chitosan were first dissolved in distilled water at 0.5% (w/v). The solutions were then sterile filtered (Corning Filter System 0.22μm membrane pores; low protein binding), frozen at -20 ^{o}C, and then placed onto a lyophilizer (SP Scientific) for a week. After lyophilization, the sterile alginate and chitosan were stored at -20^{o}C before usage. The other chemicals including AAM, MBAA, APS, TEMED, EDC and sulfo-NHS were sterilized by filtering right before usage. The sterile alginate-polyacrylamide hydrogels were synthesized following the same protocol above in a tissue culture hood. After the reaction, the hydrogels were soaked in HBSS for 30 minutes, and then rinsed three times before usage. The sterile chitosan (CL 214) was reconstituted with distilled water at 4%. The aqueous solution of EDC and sulfo-NHS at 24mg/mL was sterile filtered before mixing with the 4% sterile chitosan solution at 1:1 ratio. The mixture was used to modify the surface of the sterile alginate-polyacrylamide hydrogel immediately before application.

In Vivo Adhesion Test. Female Yorkshire swine with a bodyweight of 60-75 kg were used. All animals received humane care in accordance with the 1996 Guide for the Care and Use of Laboratory Animals recommended by the US National Institute of Health. The experimental protocol was approved by the Boston Children's Hospital Institutional Animal Care and Use Committee. The pigs were anesthetized by intramuscular injection of tiletamine/zolazepam (7 mg/kg) and xylazine (4 mg/kg), intubated with a cuffed endotracheal tube and ventilated with a volume control ventilator (Hallowell EMC Model 2000, Hallowell EMC, Pittsfield, MA) at a rate of 10-20 breaths per minute. Anesthesia was maintained with isoflurane (1-2%). Fentanyl and Buprenorphine were used for analgesia, and a maintenance IV infusion of 150-300 ml per hour was administered. The chest cavity was accessed via midline sternotomy and the pericardium was opened to expose the heart surface. TA was applied to the beating heart surface of the left ventricle and held in place to 3 minutes using a custom-made applicator. This application did not affect heart function. We attempted to peel TA off the surface of the heart while continuously recording the force used to lift it off. Videos were also recorded. In some of the experiments we added freshly drawn arterial blood to the surface of the heart prior to applying the tough adhesive in order to assess the effect of the presence of blood.

In Vitro Cell Compatibility Study. Tough adhesive (TA) and cyanoacrylate (CA) were incubated separately in 1 mL DMEM containing 10% FBS at 37 ^{o}C for 24 hours, and the adhesive masses in use were fixed at 22mg. To further assess the cell compatibility of the ingredients used to make TA, conditioned medium was also prepared by incubating the alginate-polyacrylamide hydrogel of 20mg, or 2μL mixture of 2% chitosan and 12mg/mL EDC/Sulfated NHS. Human dermal fibroblasts were plated in 96-well plates ($1.2x10^4$

cells per well, n=4 per condition). Cells were treated with each conditioned media (200 μL per well) and incubated for 24 hours at 37ºC and 5% CO_2. Cell viability was determined with a LIVE/DEAD Viability/Cytotoxicity kit for mammalian cells (Thermo Fisher Scientific). An Olympus IX81 inverted microscope was used to image live cells with excitation/emission at 495nm/515nm, and dead cells at 495nm/635nm separately.

In Vivo Biocompatibility and Stability Test. Endotoxin-free alginate and chitosan were used for the in vivo studies. The experiments were carried out in accordance with the Harvard University Standing Committee on the Use of Animals in Research and Teaching.

Subcutaneous Implantation. This study was carried out with Female Sprague Dawley rats (175-200g). Two dorsal skin incisions were conducted and two subcutaneous pockets were created by blunt preparation per animal. Tough adhesives (TA), cyanoacrylate (CA) and COSEAL (Baxter) were implanted into the dorsal subcutaneous pockets (n=4 for TA and CA; n=6 for COSEAL). The implanted materials were 200-400 mg. The skin incisions were closed with wound staples, and the animals were returned to their cages after recovery from anesthesia. At 2 weeks, the animals were euthanized by CO_2 inhalation, and the implants as well as the surrounding tissue were explanted and further processed for histological analysis. The diameters of the explants were measured with a caliper to evaluate the swelling in vivo. The samples were fixed with 4% paraformaldehyde (PFA)/PBS at 4ºC overnight, followed by rinsing with PBS for 3 times, and then processed for histology and hematoxylin and eosin (H&E) staining at the Rodent Pathology Core at Harvard Medical School. The histological sections were imaged with a Nikon E800 upright microscope. The degree of inflammation was assessed by a blinded histopathology expert.

Myocardium Attachment. This study was carried out with Female Sprague Dawley rats (225-275g). In brief, the epicardial surface was exposed and the heart was manipulated as previously described (*37*). TA or cyanoacrylate plus alginate-polyacrylamide hydrogels were compressed against the epicardial surface using a custom-made applicator to allow the adhesive to set. The incisions in the animals were closed with sutures, and animals were returned to their cages after recovery from anesthesia. Two weeks later, hearts were explanted, fixed in 4% paraformaldehyde (PFA)/PBS at 4ºC overnight, followed by rinsing with PBS for 3 times, and then processed for histology and hematoxylin and eosin (H&E) staining. The histological sections were imaged with a Nikon E800 upright microscope, from which the thickness of inflammatory region was determined. The degree of inflammation was subsequently assessed by a blinded histopathology expert.

In Vivo Stability Test. The stability of TA and their adhesion performance were evaluated by measuring the adhesion energy of TA-hydrogel interfaces after subcutaneous implantation. A lap-shear specimen was formed by compressing a

rectangular stripe of TA (15x50x1 mm^3) onto a piece of alginate-PAAm hydrogel of the same dimension. The bonding area was around 15x20 mm^2. The specimens were implanted into large dorsal subcutaneous pockets in rats following the same protocol of subcutaneous implantation above. At 2 weeks, the specimens were explanted. The adhesion energy was measured with bilayer adhesion tests described above.

Attachment of Soft Actuators on Myocardium. A soft actuator was fabricated following a protocol reported previously, which was used to support heart function (*38*). To attach the actuator onto a myocardium surface, it was first sandwiched with two sheets of TA that bonded together to fully encapsulate the device, and then compressed onto a myocardium surface of a porcine heart. The device was actuated with a pneumatic scheme following the previous protocol (*38*). The interface between the TA and the heart was examined for debonding or rupture during actuation. Videos were recorded.

Attachment of Tough Adhesive to Skin. All work was done with C57BL/6J mice (female, aged 6-8 weeks; Jackson Laboratories) and was carried out in accordance with the Institute for Animal Care and Use Committee, Harvard University, and National Institutes of Health and institutional guidelines. Mice were anesthetized with isoflurane, and a region of the dorsum was shaved. Anesthesia was maintained with isoflurane (1-2%). Two pieces of TA of 6mm diameter were applied with a custom designed applicator for 2 minutes. For the use of skin wound dressing (n=4), a skin wound was created with a biopsy punch of 4 mm on the dorsum. The tough adhesive of 10mm diameter was applied with compression for 2 minutes. Tegaderm film (3M) was attached to minimize water loss and fixed onto the dorsum using suture or wound staples. The mice were returned to their cages after recovery from anesthesia. Videos were taken to assess the adhesion under the movement of mice. The attachment of the TA was monitored on day 1 and 7.

Long-Term Cyclic Tests of Heart Sealant. A fresh porcine heart was obtained from a local grocery store. A circular defect of 4mm diameter was created with biopsy punch on the atrium wall of the heart. The defect was then sealed with an 8mm-diameter disc of the tough adhesive. The heart with the attached sealant was submersed in a large reservoir of PBS. The inflation-deflation deformation of the heart was mimicked by pumping air in and out for 18 hours (22,000 cycles in total). Photos and videos were recorded to examine any leakage at the defect site.

Burst Pressure Measurements. This study was carried out by following the ASTM F2392 standard protocol for measuring burst strength of surgical sealants. Myocardium tissues of 3-5mm thickness were explanted from fresh porcine hearts purchased from a local grocery store. A 3mm-diameter hole was punched at the center of the myocardium tissue. A 15mm-diameter tough adhesive with and without gluing its back to a rigid PET

film was adhered onto the myocardium tissue. The pressure was applied by pumping PBS using a syringe pump (Harvard Apparatus PHD 2000 Dual Syringe Pump) at a rate of 2 mL/min from the bottom of the specimen. During the measurement, the pressure was recorded as a function of time and the burst pressure was identified when a burst occurred.

Cartilage Repair with Injectable TA. UV-curable alginate-polyethylene glycol diacrylate (alginate-PEGDA) hydrogel was chosen as the dissipative matrix for the injectable TA. The ultrapure alginate (MVG and VLVG at 1:1 ratio) and PEGDA (20kDa) were dissolved in distilled water at 5% and 60%, separately. The two solutions were then syringe-mixed at 1 to 1 volume ratio, and mixed with calcium sulfate slurries and I2959. The final concentrations of I2959 and calcium sulfate were 0.1% and 20mM. The adhesive was cured with UV light of wavelength 365nm (DYMAX 2000 Flood) for 10 minutes.

The kinetics of gelation was measured with DHR-3 rheometer (TA Instruments) using a 20mm stainless steel plate geometry. The UV light was applied at 20mW/cm^2 for 2 minutes by using an OmniCure S Series light curing system (Excelitas Tech. Corp.). The compressive stress-strain curves were measured by compressing 8mm-diameter discs of the injectable TA at a strain rate of 100% per minute with an Instron machine (model 3342 with load cell of maximum 1000N).

Cartilage discs of 8mm diameter were explanted from porcine articular cartilage. The cartilage specimen was first compressed by the Instron machine to 20% strain to extract the original stress-strain curves. After the compression, a 4mm-diameter hole was created in the middle of the specimen to create a defect, followed by the second run of compression. The injectable TA was then applied to repair the cartilage defect; a third run of compression was performed to assess the compressive performance after repair.

Hepatic Hemorrhage Model. This study, involving Female Sprague Dawley rats (175-200g), was carried out in accordance with the Institute for Animal Care and Use Committee, Harvard University. Liver laceration was performed to create an uncontrolled hemorrhage condition in rats, as per previous reports in the literature (*39, 40*). In brief, the animals were anesthetized via isoflurane by inhalation (4%), and then by ventilation (2%). A ventral midline laparotomy incision was performed, and the left lobe of the liver was exposed. A nearly full-thickness wound was created with a biopsy punch of 6mm, followed by laceration with a scissor. Immediately after injury, TA or the hemostatic matrix SURGIFLO (Ethicon; as a positive control) was applied on the lesion site (N=4). Compression was applied on TA and liver with spatulas. Untreated animals were included for negative control (N=4). During the surgery, the blood was carefully collected with filter papers at time points of 2, 5 and 10 minutes. The total amount of the blood loss at each time point was determined by weighing the papers and recorded. The

abdomen was closed in 15 minutes after the wound creation and treatment. The animals were allowed to recover from anesthesia before returning to the cage. The animals were monitored to check secondary hemorrhage. At 2 weeks, the animals were euthanized by CO_2 inhalation, and the livers were explanted and further processed for histological analysis. The samples were fixed with 4% paraformaldehyde (PFA)/PBS at 4^{o}C for 2 days, followed by rinsing with PBS for 3 times, and then processed for histology and hematoxylin and eosin (H&E) staining at the Rodent Pathology Core at Harvard Medical School. The histological sections were imaged with a Nikon E800 upright microscope.

Supplementary Text

Effects of Coupling Reagents on Adhesion. The importance of building strong chemical bonds for interfacial bridging was examined by comparing TA with adhesives that were modified with either the coupling reagents or the bridging polymer alone (Fig. S5). EDC was applied at very low concentration (~0.1% by weight of TA); this undergoes fast hydrolysis (half-life time ~10 minutes) in aqueous solutions (*22*). The use of the coupling reagents EDC/Sulfo-NHS alone led to very low adhesion energy (14 Jm^{-2}); without the bridging polymer, the dissipative matrix is likely to be repelled electrostatically by the negatively charged tissue surfaces. The bridging polymer without the coupling reagents led to moderate adhesion energy (303 Jm^{-2}). The purely electrostatic attraction in this situation is not as strong as covalent bonds in bridging the two surfaces. In contrast, the tough adhesive consisting of both the bridging polymer and the coupling reagents led to high adhesion energy (1121 Jm^{-2}).

Comparison between TA and Existing Adhesives. Figure S7 summarizes the adhesion energy and the matrix toughness of a variety of adhesives that are used in the clinic or under development, as well as cartilage. Many commercially available adhesives such as fibrin glues and COSEAL have low adhesion energy and low matrix toughness. They often comprise a brittle matrix (*11, 13, 27*), which can cause debonding due to cohesive failure of the adhesive matrix, as the low matrix toughness sets the upper bound for the adhesion energy. Adhesive bandages, despite a tough elastomer matrix, rely on very weak interaction with tissues, leading to high matrix toughness but low adhesion energy. Our design enables TA to combine high adhesion energy and high matrix toughness simultaneously, which leads to properties that rival cartilage.

Adhesion of TA to Hydrogels. The toughness of the substrates to which TA adheres will set an upper bound for the adhesion energy. Indeed, when a tough hydrogel like alginate-polyacrylamide hydrogel was used as the substrate, TA achieved adhesion energy on the order of 1000 Jm^{-2}. Alternatively, the adhesion energy was similar to the bulk toughness of the substrate, if the substrate toughness was lower than 1000 Jm^{-2} (for example,

adhesion to PAAm hydrogels) (Figs. S8 and S9).

Injectable Adhesives for Cartilage Repair. The design of tough adhesive can be extended to injectable hydrogels. We chose alginate-polyethylene glycol diacrylate hydrogels as the dissipative matrix for injectable TA. The pregel solution can be injected via syringe into a defect site, and formed a tough matrix upon exposure to UV light. The injectable TA sustained a large compressive stress (6.6MPa) without rupture (Fig. S19). Due to this robust compressive property, the injectable TA was used to repair a cylindrical defect in explanted cartilage discs. The defect surface was first casted with the mixture of the bridging polymer and the coupling reagents for interfacial bridging, followed by injection and UV-curing of the injectable TA. Strong adhesion formed between the adhesive and surrounding tissues (Fig. S20). The results showed that no debonding or rupture of the TA was observed after compression testing, indicative of strong adhesion and tough matrix; the compressive property of the repaired cartilage was restored as compared to untreated tissues.

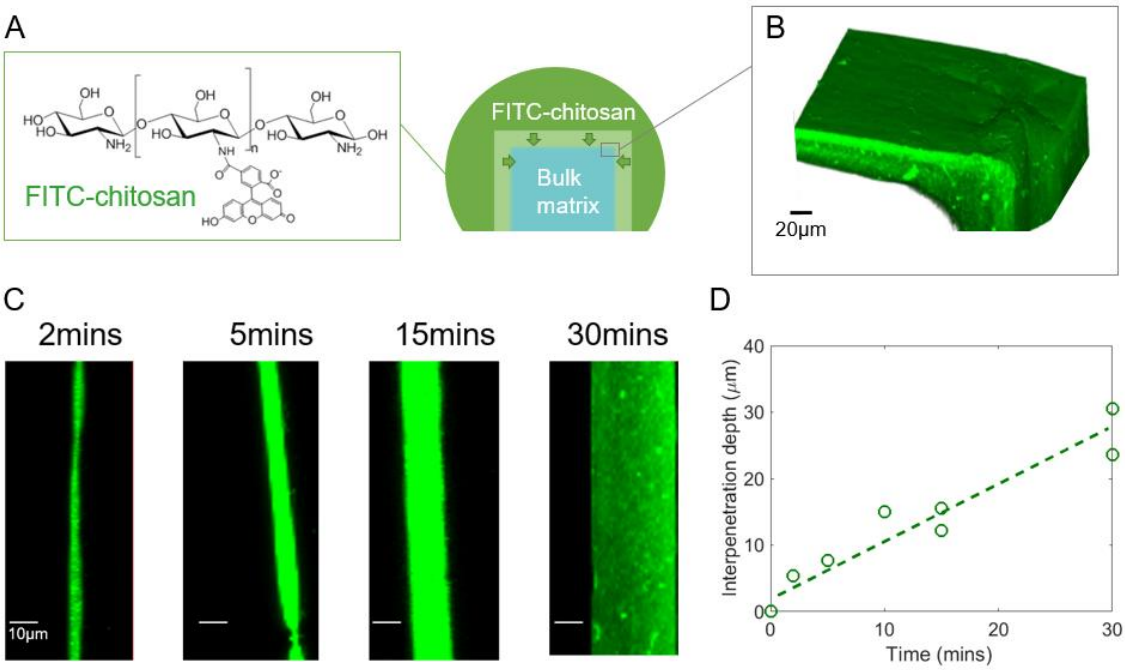

Fig. S1

Physical interpenetration of bridging polymer into bulk matrix. (**A**) FITC-chitosan was applied to alginate/polyacrylamide hydrogel, and allowed to diffuse into the matrix. (**B**) Diffusion of FITC-chitosan over time was imaged by confocal fluorescence microscopy. Scale bar, 20 μm. (**C**) Images of the adhesive surface containing FITC-chitosan at different incubation times. Scale bar, 10μm. (**D**) Interpenetration depth increased with the incubation time.

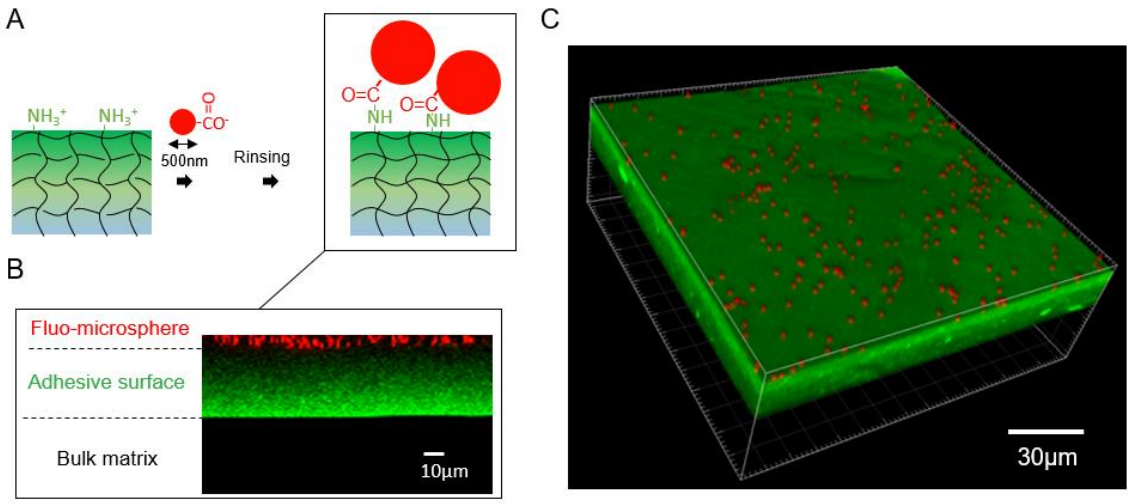

Fig. S2

Retention of fluorescent microspheres on TA. (**A**) Schematic showing that fluorescent microspheres of 500nm diameter (red) are spread on TA consisting of FITC-chitosan (green), and after rinsing with PBS repeatedly, the microspheres remain on the tough adhesive via electrostatic attraction and formation of amide bonds. (**B**) 2D cross-section image of the sandwich structure: fluorescent microspheres (red), FITC-chitosan interpenetrating adhesive surface (green) and bulk matrix of the tough adhesive (from top to bottom). As the microsphere size is larger than the mesh size of the tough adhesive (on the order of 10 nm), the microspheres remain on the outer surface. (**C**) 3D construct of TA with FITC-chitosan and fluorescent microspheres attached on the surface. Scale bar, 30μm.

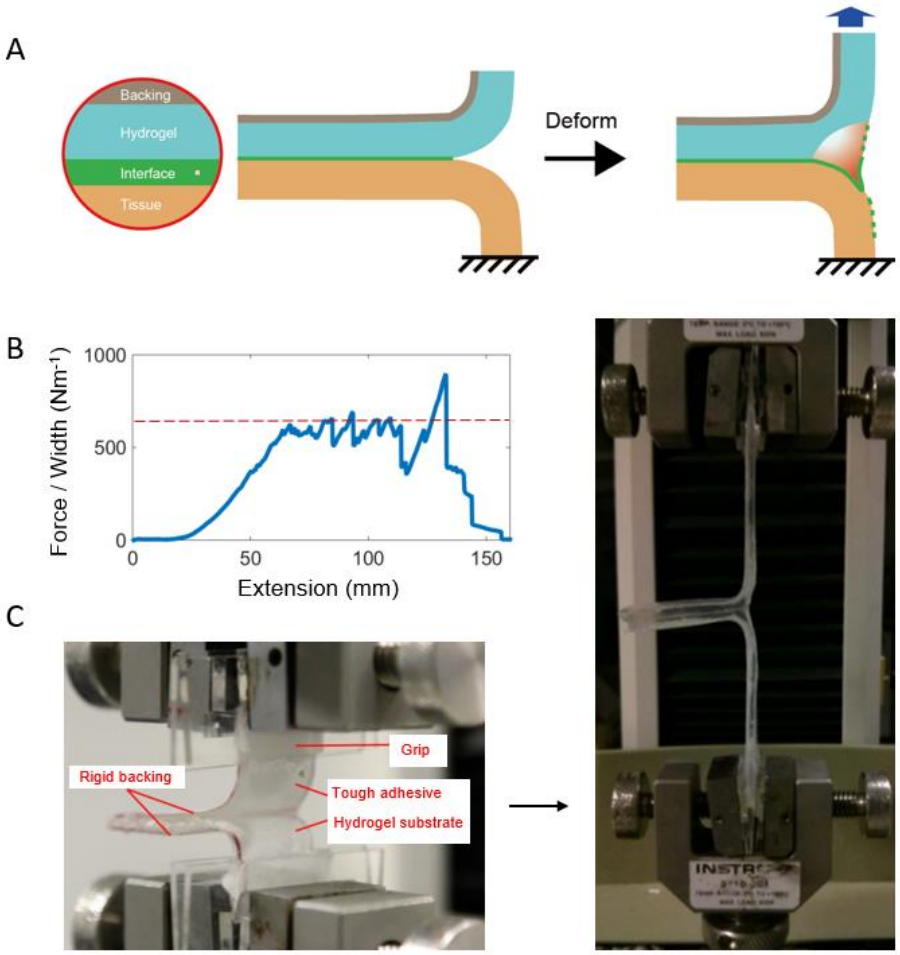

Fig. S3

Peeling adhesion test. (**A**) Schematics of TA-tissue specimen for adhesion measurements, in which one side of the TA was glued to a rigid plastic film as a backing layer, to eliminate energy dissipation in regions away from the crack tip. Two free arms of TA-tissue bilayer specimen were stretched with an Instron machine in 180-degree peeling test. (**B**) Adhesion energy was determined as two times the plateau value of the force per width required for extension, when the crack propagates under steady state (red dashed line). (**C**) Digital photos showing the TA-hydrogel specimen under peeling test.

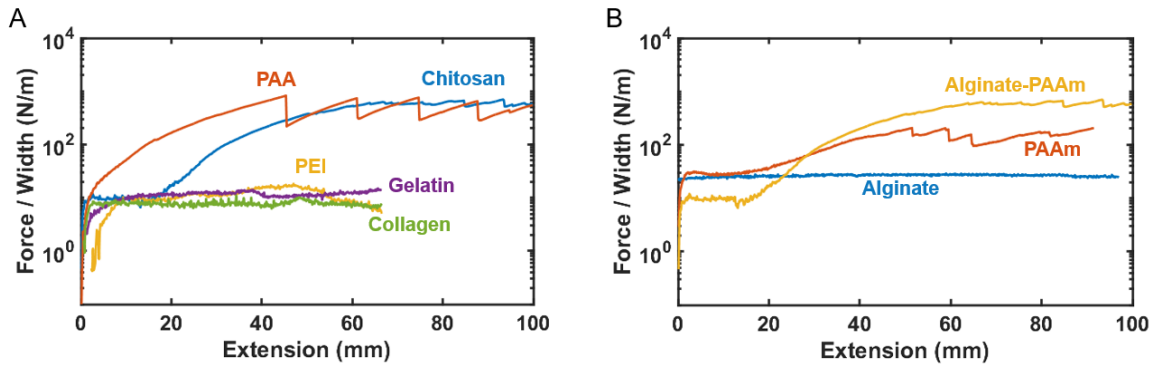

Fig. S4

Force-extension curves of peeling tests. Adhesion energy was calculated based on the average value of force/width at the plateau. (**A**) Tested polymers include chitosan, polyallylamine (PAA), polyethylenimine (PEI), gelatin and collagen. (**B**) Tested hydrogel matrix used to make adhesives include alginate, polyacrylamide (PAAm) and alginate-PAAm hydrogels.

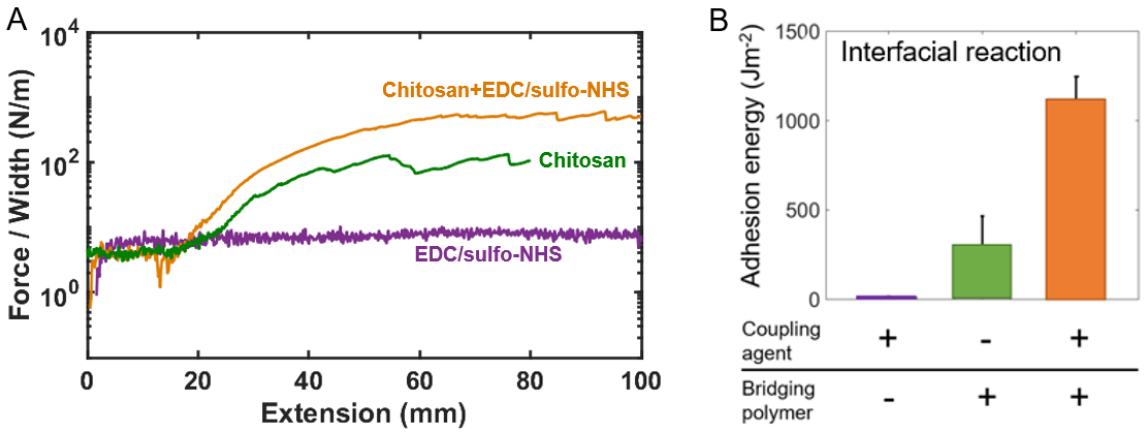

Fig. S5

Effects of interfacial reaction on adhesion. The alginate-polyacrylamide hydrogel served as the dissipative matrix. Chitosan and EDC/sulfo-NHS were used as the bridging polymer and coupling reagents, respectively. Adhesion energy was calculated based on the average value of force/width at the plateau. (**A**) Force-extension curves of peeling tests. (**B**) Measured adhesion energy to porcine skin. Error bars show standard deviation; N=4.

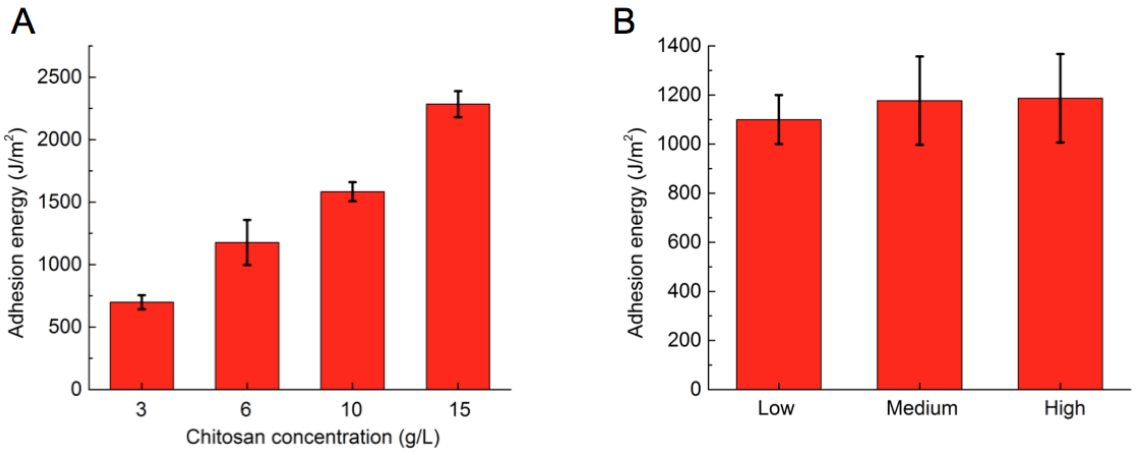

Fig. S6

Effects of concentration and molecular weight of chitosan on adhesion energy. TA was applied onto an alginate-polyacrylamide hydrogel, followed by peeling adhesion tests. The concentration (**A**) and molecular weight (**B**) of chitosan were varied in making the TA. Error bars show standard deviation; N=4.

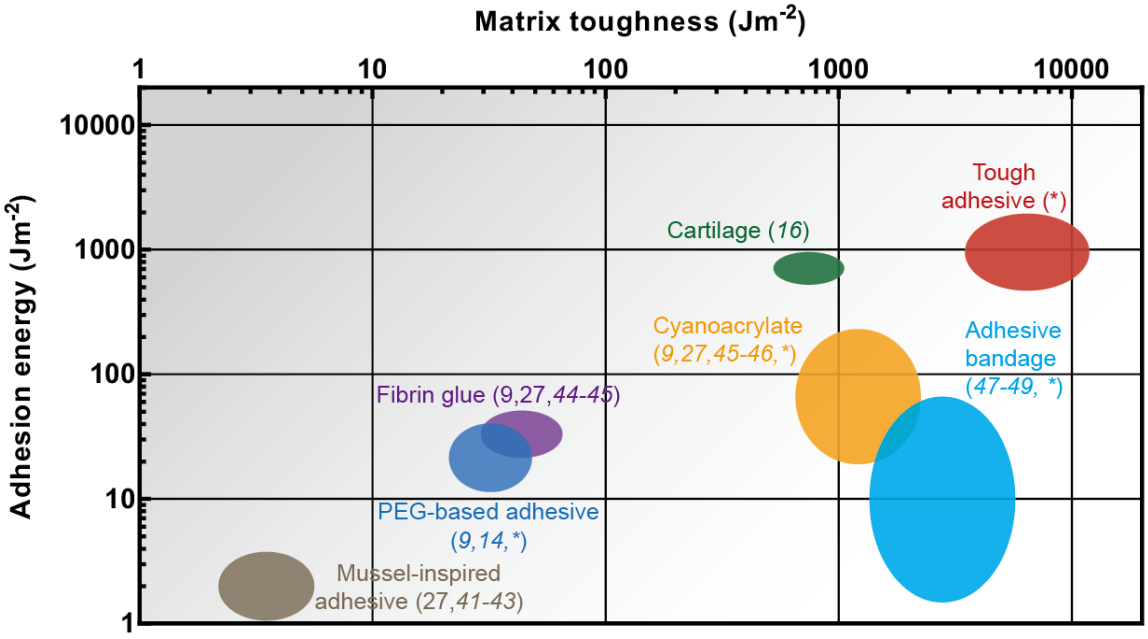

Fig. S7

Comparison of adhesion energy and matrix toughness of various adhesives and cartilage. The references used to extract the data are as labelled (*9, 14, 16, 27, 41-49*). The data obtained with our measurements is labeled with asterisks (*24*).

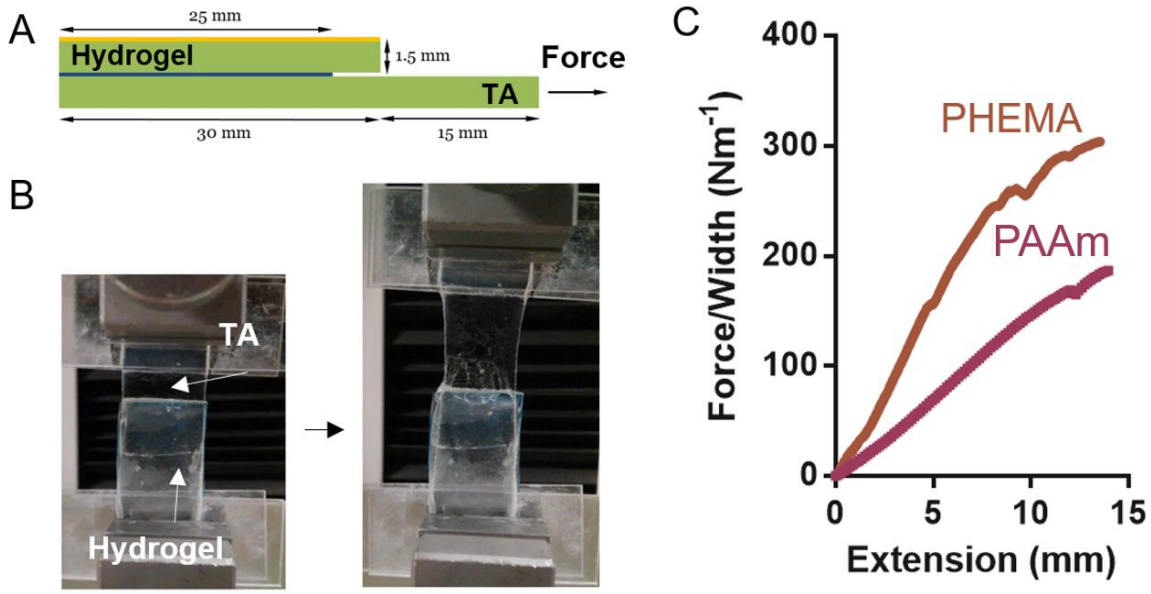

Fig. S8

Bilayer adhesion test. (A) Schematic of a bilayer adhesion specimen comprising TA and a hydrogel with one side bonded to a rigid plastic film (labelled in yellow). Polyacrylamide hydrogel (PAAm) and poly(hydroxyethyl methacrylate) hydrogel (PHEMA) were tested. The free arm of TA was stretched by an Instron machine. (**B**) Digital photos of a bilayer adhesion specimen before and after debonding. (**C**) Force-extension curves of the TA-PAAm and TA-PHEMA specimens, which end when a pre-existing crack starts to propagate.

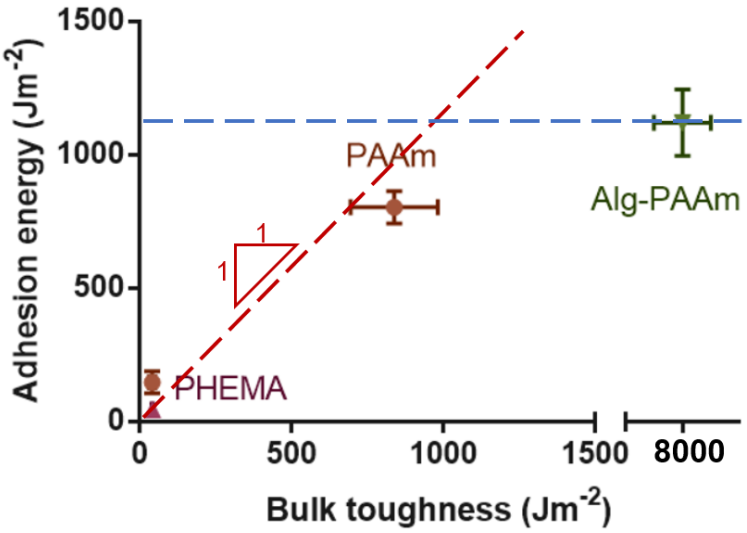

Fig. S9

Correlation between adhesion energy and bulk toughness of the hydrogel substrates to which TA adheres. Polyhydroxyethyl methacrylate hydrogels (PHEMA), alginate-PAAm hydrogels (Alg-PAAm) and polyacrylamide hydrogels (PAAm) were tested. The PAAm hydrogels were prepared with 2 levels of bulk toughness. The red dashed line indicates that the adhesion energy equals to the bulk toughness of the hydrogels, and the blue dashed line indicates the maximum adhesion energy obtained with TA. Error bars show standard deviation; N=4.

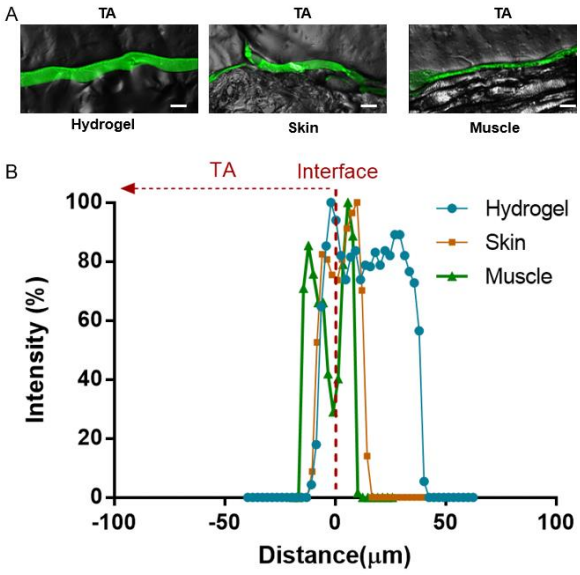

Fig. S10

Bridging polymer at interface. (**A**) Confocal images of cryosections of TA-polyacrylamide hydrogel, TA-skin and TA-muscle interfaces. The images include bright field signals and green fluorescence from FITC-chitosan. Scale bar, 50μm. (**B**) Fluorescent intensity profile across the interfaces, where the location of interface is marked with a red dashed line and the TA is positioned on the left side.

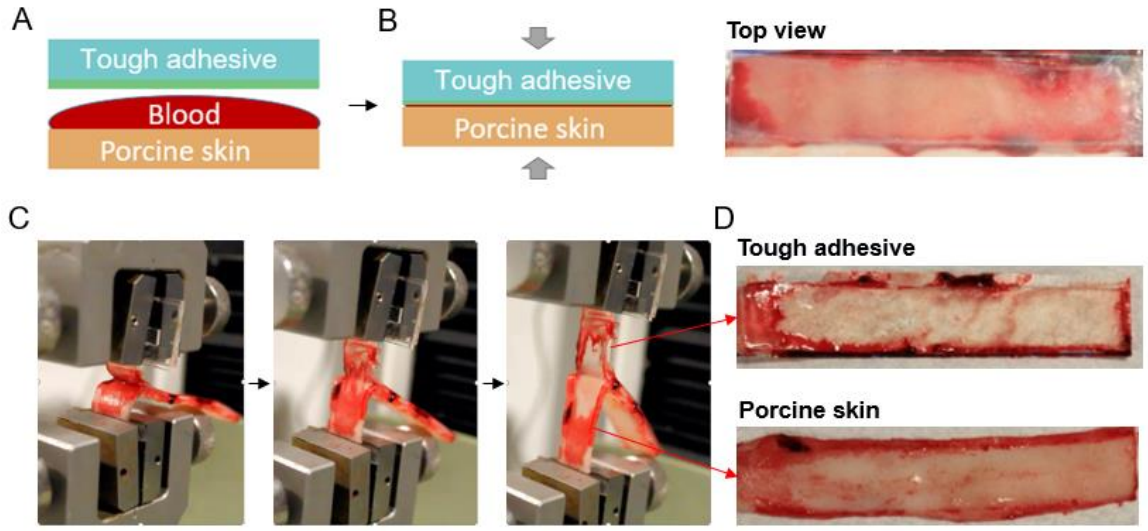

Fig. S11

Adhesion formation with exposure to blood. (**A**) Effect of blood exposure was evaluated by covering the whole surface of porcine skin with whole blood, before TA was applied. (**B**) Adhesion is formed by compressing TA onto the skin. (**C**) The specimen was stretched with an Instron machine at a constant rate of 100 mm/min, while the side of the tough adhesive was glued to a rigid plastic film to concentrate energy dissipation at the crack. During the stretching, fibrillar structures were observed at the crack tip, indicative of large deformation and effective energy dissipation. (**D**) After debonding, the surfaces of TA and skin was examined for debris of adhesive particles and blood residues.

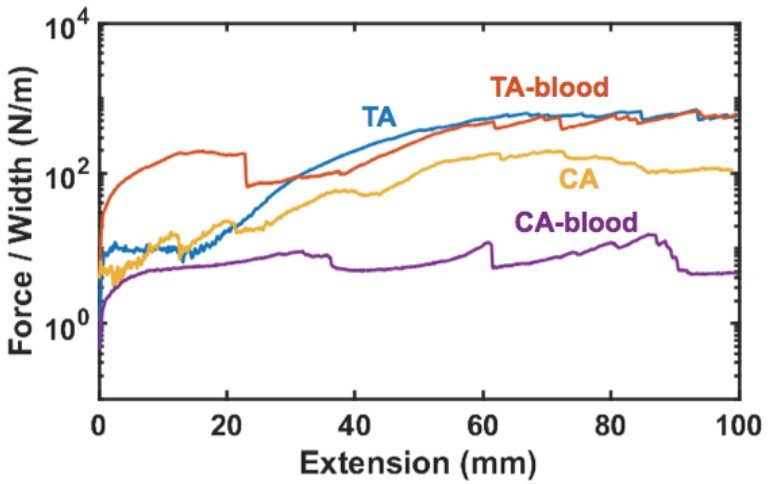

Fig. S12

Force-extension curves of peeling tests. The adhesion energy was calculated based on the average value of force/width at the plateau region. The tough adhesive (TA) and cyanoacrylate (CA) were applied onto the porcine skin with and without exposure to blood on porcine skin surface.

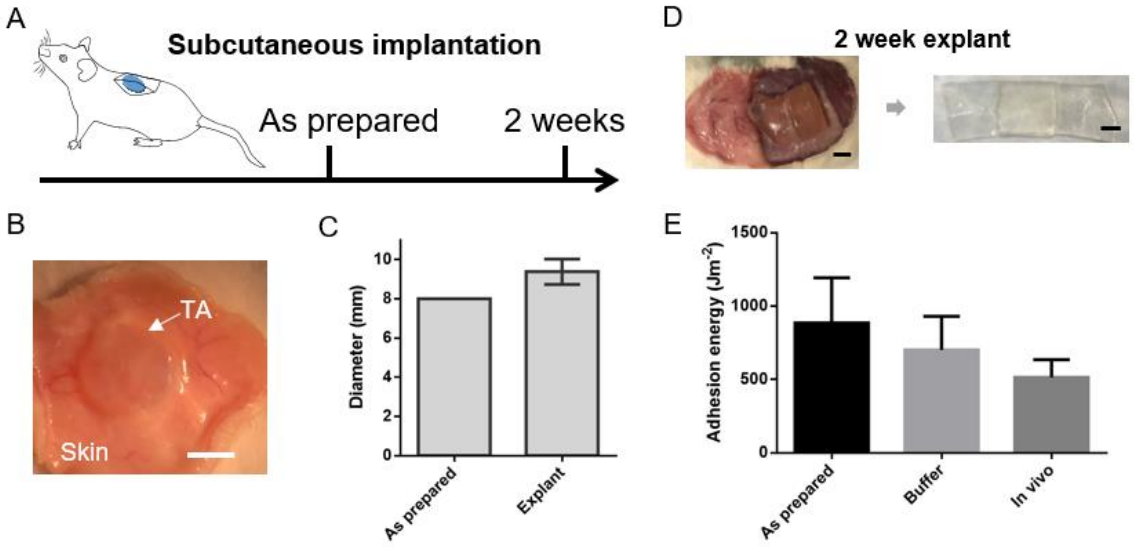

Fig. S13

Adhesion was maintained over time in vivo. (**A**) Schematic and timeline for subcutaneous implantation in rats. (**B**) Digital photo of TA with surrounding tissues. Scale bar, 5mm. (**C**) Diameters before and after implantation. (**D**) Digital photos of a bilayer adhesion specimen that was implanted in vivo for 2 weeks. The specimen was formed with TA and alginate-polyacrylamide hydrogel. Scale bar, 10mm. (**E**) Adhesion energy of specimens as prepared, after being soaked in DMEM buffer for 2 weeks, or after being implanted in vivo for 2 weeks. Error bars show standard deviation; N=4.

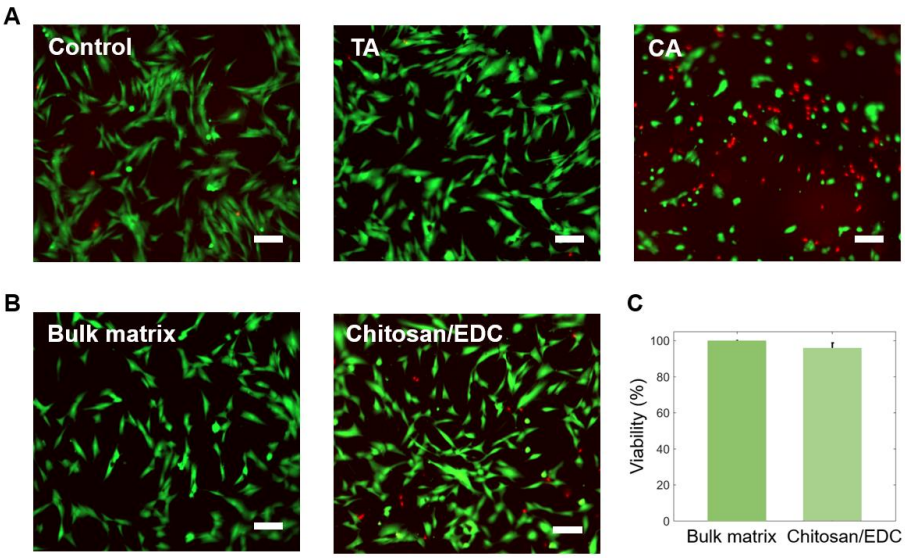

Fig. S14

In vitro cell compatibility. (**A**) Fluorescent images of human dermal fibroblasts after 24-hour culture in mediums that were conditioned with TA, CA or DMEM as control. (**B**) Fluorescent images of cells in mediums that were conditioned with the bulk matrix, or the mixture of chitosan/EDC. Scale bar, 100μm. (**C**) Cell viability was compared between the conditions by quantifying the percentage of live cells (viability). Error bars show standard deviation; N=4.

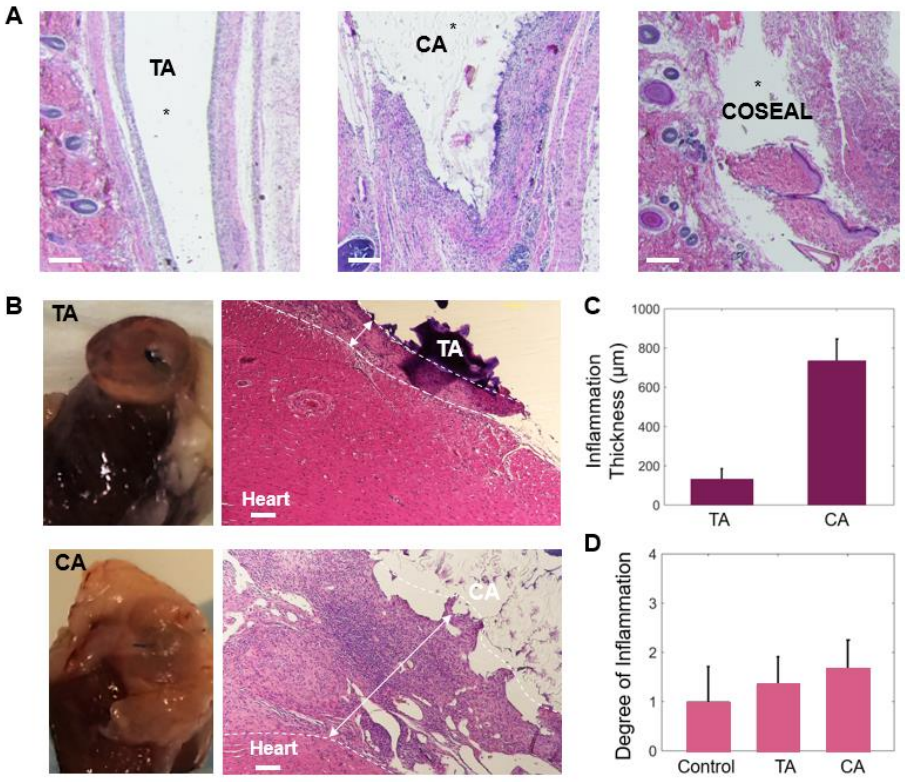

Fig. S15

In vivo biocompatibility. (**A**) Histological sections of implants (labeled with asterisks) and surrounding tissues. TA, CA and COSEAL (from Baxter) were implanted into rats subcutaneously for 2 weeks. Scale bar, 200μm. (**B**) Images and histological sections of TA and CA attached onto the rat myocardium for 2 weeks. CA elicits more fibrosis than TA. Scale bar, 100μm. (**C**) Thickness of inflammatory region measured from histological sections. Error bars show standard deviation; N=3. (**D**) Degree of inflammation was determined by a pathologist (blinded analysis) for all three conditions (0=normal, 1=very mild, 2=mild, 3=moderate, 4=severe, 5=very severe).

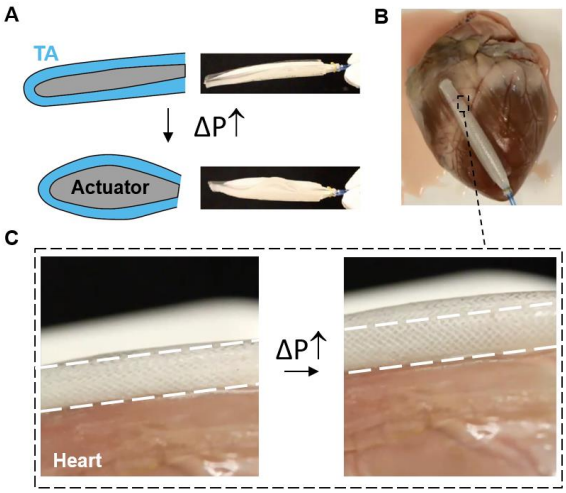

Fig. S16

Encapsulation and attachment of soft actuators with TA onto myocardium surface. (**A**) An actuator was encapsulated with TA and functioned properly. (**B**) TA anchored the actuator onto a porcine heart. (**C**) TA accommodated the deformation of the attached actuators without debonding or rupture during actuation.

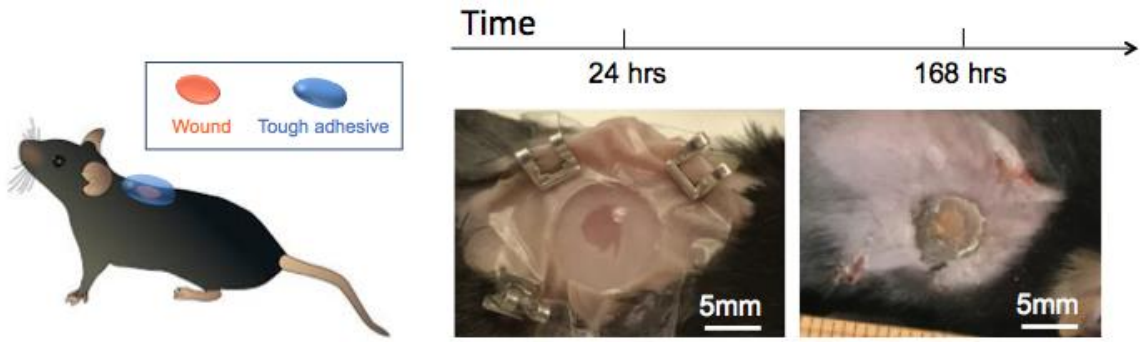

Fig. S17

Use of TA as skin wound dressing. A 10mm disc of TA was attached on the dorsum of mice, where a skin wound of 4mm diameter was created with biopsy punch. Adhesion was inspected at 24 and 168 hours. Although the adhesive dried by 168 hours, the TA remained strongly adherent to the skin. Scale bar, 5mm.

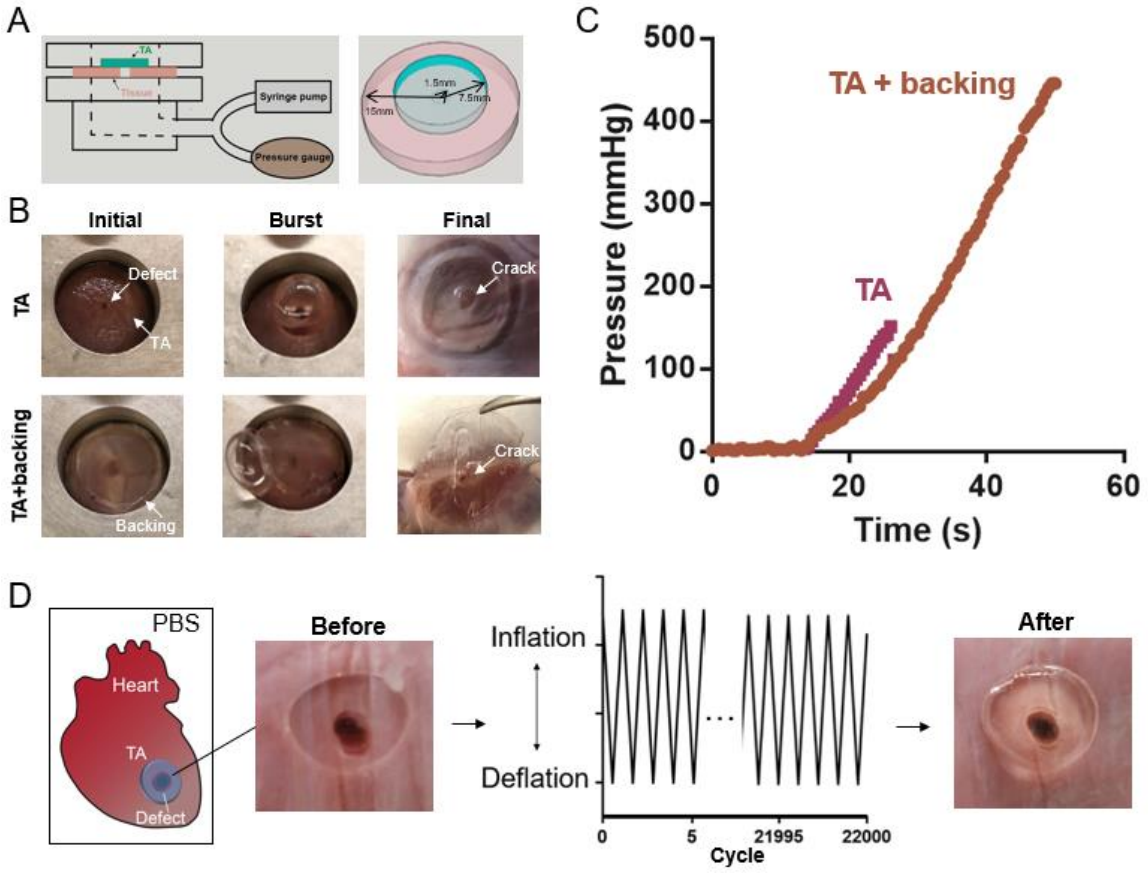

Fig. S18

Performance of TA heart sealants. (**A**) Experimental setup and specimen dimensions for the burst pressure measurement. PBS was pumped into the specimen chamber under a constant flow rate of 2 mL/min, while the pressure was recorded with a pressure gauge. (**B**) Images of the TA-myocardium specimen before and after burst. A rigid PET film was attached to the back of TA sealant. The pathway of crack propagation after burst indicated cohesive failure of the sealant with minimal debonding at interface. (**C**) Pressure-time curves of the TA sealant with and without backing, which end at the time point when a burst occurs. (**D**) Schematic and photos of the TA sealant before and after a long-term reliability tests. The repaired heart was inflated/deflated with pressurized air for 22,000 cycles while being immersed in PBS for 18 hours.

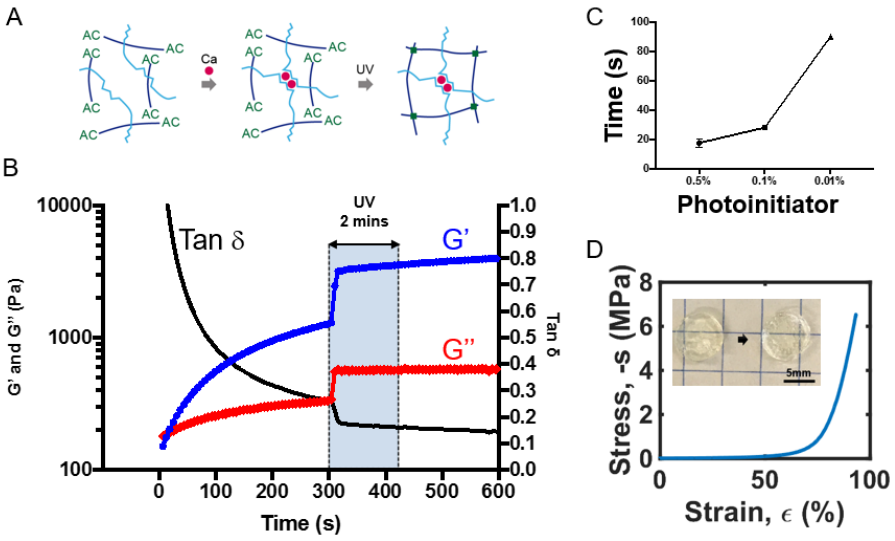

Fig. S19

Gelation and compressive properties of injectable TA. UV-curable polyethylene glycol (PEG)-alginate hydrogels serve as the dissipative matrix for the injectable TA. (**A**) Schematic of two-step gelation process, in which the alginate (light blue lines) is cross-linked with calcium ions (red circles) and the PEG network (dark blue lines) is formed when the UV light triggers the cross-linking reaction between acrylate (AC) functional groups on PEG chains. (**B**) Kinetics of shear modulus (storage modulus G' and loss modulus G'') and loss angle (tan δ) versus time. (**C**) Effects of the photoinitiator (I2959) concentration on the gelation time of the PEG network. (**D**) Compressive stress-strain curves of the injectable TA. The inset shows the specimens before and after the compression test where the maximum compressive stress was 6.6 MPa.

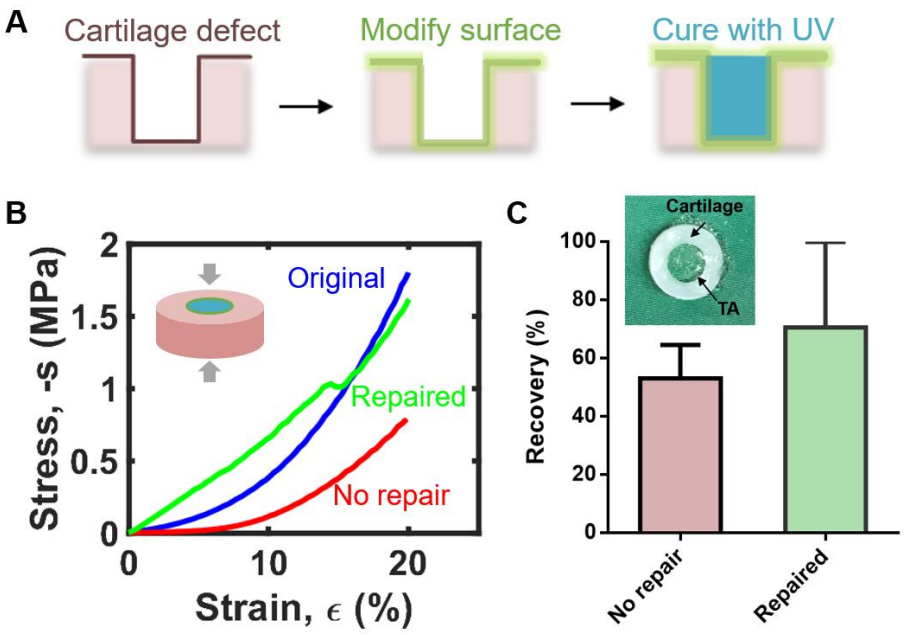

Fig. S20

In vitro demonstration using an injectable TA to repair a cartilage defect. (**A**) The site of application is treated with chitosan and EDC/sulfo-NHS for interfacial bridging, filled with pregel solution and then exposed immediately to UV for rapid gelation. (**B**) Compressive stress-strain curves of the cartilage explant before and after repair. (**C**) The recovery was evaluated by the ratio of stress levels at 20% strains. The inset is a photo of cartilage disc repaired with TA. N=3.

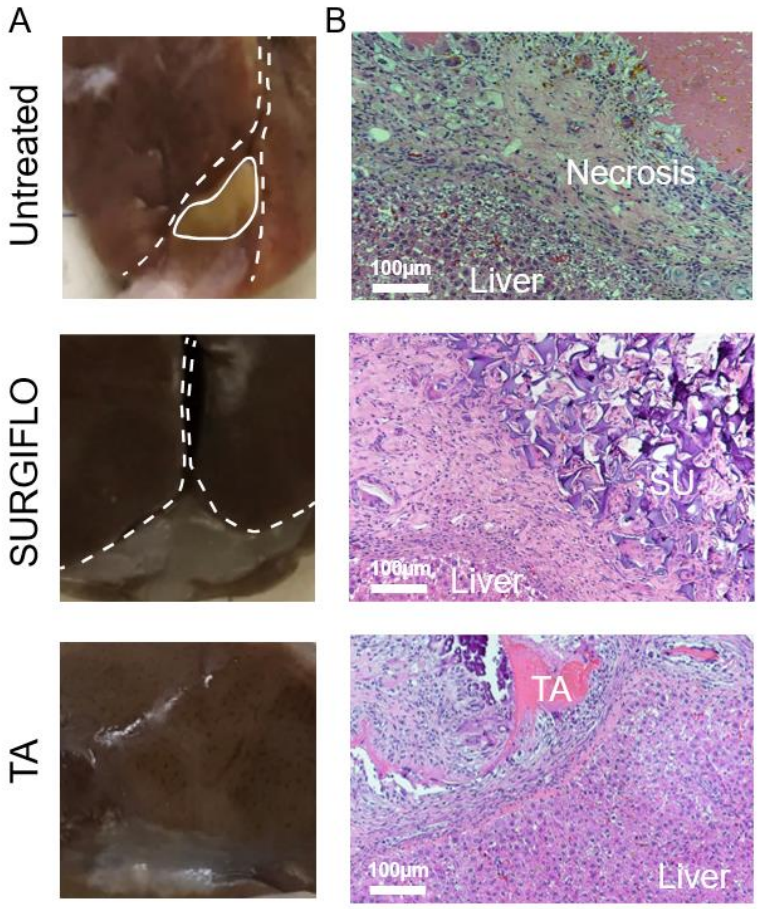

Fig. S21

Digital photos of explanted livers and corresponding histological sections. (**A**) Digital photos of the livers explanted from the rats that were untreated, or treated with a commercial hemostat SURGIFLO and with TA. The boundaries of multiple lobes of the livers that adhered to the lesion sites are marked with white dashed lines. The area of necrosis is marked with white solid lines. (**B**) Histological sections of the explanted livers and implants at the lesion sites, in which the locations of necrossi, TA and SURGIFLO (SU) are marked.

Movie S1

3D construct of tough adhesive (TA). TA consists of an adhesive surface containing FITC-chitosan in which fluorescent microspheres of 500nm diameter were immobilized.

Movie S2

Peeling test of TA adherent on porcine skin. TA was applied on a piece of porcine skin that was first covered with blood, followed by 180-degree peeling test.

Movie S3

In vivo adhesion test. A ribbon of TA was applied to a beating porcine heart, followed by a peeling test in vivo.

Movie S4

Attachment of TA on skin. Two pieces of TA were applied to the epidermis of mice, and the adhesion was inspected as the animal moved.

Movie S5

TA sealant under static and cyclic deformation. A piece of TA was used to seal a defect on a porcine heart, and prevented leakage during thousands cycles of heart inflation-deflation.

Movie S6

Burst pressure test of TA sealant. TA with and without a plastic backing film were attached onto myocardium tissues and subject to pressurized saline till a burst occurred.

References and Notes

1. S. Duflo, S. L. Thibeault, W. Li, X. Z. Shu, G. D. Prestwich, Vocal fold tissue repair in vivo using a synthetic extracellular matrix. *Tissue Eng.* **12**, 2171–2180 (2006). doi:10.1089/ten.2006.12.2171 Medline

2. B. Sharma, S. Fermanian, M. Gibson, S. Unterman, D. A. Herzka, B. Cascio, J. Coburn, A. Y. Hui, N. Marcus, G. E. Gold, J. H. Elisseeff, Human cartilage repair with a photoreactive adhesive-hydrogel composite. *Sci. Transl. Med.* **5**, 167ra6 (2013). doi:10.1126/scitranslmed.3004838 Medline

3. M. R. Prausnitz, R. Langer, Transdermal drug delivery. *Nat. Biotechnol.* **26**, 1261–1268 (2008). doi:10.1038/nbt.1504 Medline

4. J. Li, D. J. Mooney, Designing hydrogels for controlled drug delivery. *Nat. Rev. Mater.* **1**, 16071 (2016). doi:10.1038/natrevmats.2016.71

5. C. Ghobril, K. Charoen, E. K. Rodriguez, A. Nazarian, M. W. Grinstaff, A dendritic thioester hydrogel based on thiol-thioester exchange as a dissolvable sealant system for wound closure. *Angew. Chem. Int. Ed.* **52**, 14070–14074 (2013). doi:10.1002/anie.201308007 Medline

6. M. W. Grinstaff, Designing hydrogel adhesives for corneal wound repair. *Biomaterials* **28**, 5205–5214 (2007). doi:10.1016/j.biomaterials.2007.08.041 Medline

7. E. T. Roche, R. Wohlfarth, J. T. B. Overvelde, N. V. Vasilyev, F. A. Pigula, D. J. Mooney, K. Bertoldi, C. J. Walsh, A bioinspired soft actuated material. *Adv. Mater.* **26**, 1200–1206 (2014). doi:10.1002/adma.201304018 Medline

8. R. Feiner, L. Engel, S. Fleischer, M. Malki, I. Gal, A. Shapira, Y. Shacham-Diamand, T. Dvir, Engineered hybrid cardiac patches with multifunctional electronics for online monitoring and regulation of tissue function. *Nat. Mater.* **15**, 679–685 (2016). doi:10.1038/nmat4590 Medline

9. K. A. Vakalopoulos, Z. Wu, L. Kroese, G.-J. Kleinrensink, J. Jeekel, R. Vendamme, D. Dodou, J. F. Lange, Mechanical strength and rheological properties of tissue adhesives with regard to colorectal anastomosis: An ex vivo study. *Ann. Surg.* **261**, 323–331 (2015). doi:10.1097/SLA.0000000000000599 Medline

10. H. V. Vinters, K. A. Galil, M. J. Lundie, J. C. Kaufmann, The histotoxicity of cyanoacrylates. A selective review. *Neuroradiology* **27**, 279–291 (1985). doi:10.1007/BF00339559 Medline

11. S. Rose, A. Prevoteau, P. Elzière, D. Hourdet, A. Marcellan, L. Leibler, Nanoparticle solutions as adhesives for gels and biological tissues. *Nature* **505**, 382–385 (2014). doi:10.1038/nature12806 Medline

12. D. G. Barrett, G. G. Bushnell, P. B. Messersmith, Mechanically robust, negative-swelling, mussel-inspired tissue adhesives. *Adv. Healthc. Mater.* **2**, 745–755 (2013). doi:10.1002/adhm.201200316 Medline

13. D. H. Sierra, Fibrin sealant adhesive systems: A review of their chemistry, material properties and clinical applications. *J. Biomater. Appl.* **7**, 309–352 (1993). doi:10.1177/088532829300700402 Medline

14. D. G. Wallace, G. M. Cruise, W. M. Rhee, J. A. Schroeder, J. J. Prior, J. Ju, M. Maroney, J. Duronio, M. H. Ngo, T. Estridge, G. C. Coker, A tissue sealant based on reactive multifunctional polyethylene glycol. *J. Biomed. Mater. Res.* **58**, 545–555 (2001). doi:10.1002/jbm.1053 Medline

15. A. K. Dastjerdi, M. Pagano, M. T. Kaartinen, M. D. McKee, F. Barthelat, Cohesive behavior of soft biological adhesives: Experiments and modeling. *Acta Biomater.* **8**, 3349–3359 (2012). doi:10.1016/j.actbio.2012.05.005 Medline

16. M. Moretti, D. Wendt, D. Schaefer, M. Jakob, E. B. Hunziker, M. Heberer, I. Martin, Structural characterization and reliable biomechanical assessment of integrative cartilage repair. *J. Biomech.* **38**, 1846–1854 (2005). doi:10.1016/j.jbiomech.2004.08.021 Medline

17. J. M. Pawlicki, L. B. Pease, C. M. Pierce, T. P. Startz, Y. Zhang, A. M. Smith, The effect of molluscan glue proteins on gel mechanics. *J. Exp. Biol.* **207**, 1127–1135 (2004). doi:10.1242/jeb.00859 Medline

18. A. M. Wilks, S. R. Rabice, H. S. Garbacz, C. C. Harro, A. M. Smith, Double-network gels and the toughness of terrestrial slug glue. *J. Exp. Biol.* **218**, 3128–3137 (2015). doi:10.1242/jeb.128991 Medline

19. M. Braun, M. Menges, F. Opoku, A. M. Smith, The relative contribution of calcium, zinc and oxidation-based cross-links to the stiffness of *Arion subfuscus* glue. *J. Exp. Biol.* **216**, 1475–1483 (2013). doi:10.1242/jeb.077149 Medline

20. J. Y. Sun, X. Zhao, W. R. K. Illeperuma, O. Chaudhuri, K. H. Oh, D. J. Mooney, J. J. Vlassak, Z. Suo, Highly stretchable and tough hydrogels. *Nature* **489**, 133–136 (2012). doi:10.1038/nature11409 Medline

21. N. Nakajima, Y. Ikada, Mechanism of amide formation by carbodiimide for bioconjugation in aqueous media. *Bioconjug. Chem.* **6**, 123–130 (1995). doi:10.1021/bc00031a015 Medline

22. M. A. Gilles, A. Q. Hudson, C. L. Borders Jr., Stability of water-soluble carbodiimides in aqueous solution. *Anal. Biochem.* **184**, 244–248 (1990). doi:10.1016/0003-2697(90)90675-Y Medline

23. J. G. Fernandez, S. Seetharam, C. Ding, J. Feliz, E. Doherty, D. E. Ingber, Direct bonding of chitosan biomaterials to tissues using transglutaminase for surgical repair or device implantation. *Tissue Eng. Part A* **23**, 135–142 (2017). doi:10.1089/ten.tea.2016.0266 Medline

24. Materials and methods are available as supplementary materials.

25. A. N. Gent, Adhesion and strength of viscoelastic solids. Is there a relationship between adhesion and bulk properties? *Langmuir* **12**, 4492–4496 (1996). doi:10.1021/la950887q

26. J. W. Hutchinson, Z. Suo, Mixed mode cracking in layered materials. *Adv. Appl. Mech.* **29**, 63–191 (1992).

27. H. Yuk, T. Zhang, S. Lin, G. A. Parada, X. Zhao, Tough bonding of hydrogels to diverse non-porous surfaces. *Nat. Mater.* **15**, 190–196 (2016). doi:10.1038/nmat4463 Medline

28. T. Stefanov, B. Ryan, A. Ivanković, N. Murphy, Mechanical bulk properties and fracture toughness of composite-to-composite joints of an elastomer-toughened ethyl cyanoacrylate adhesive. *Int. J. Adhes. Adhes.* **68**, 142–155 (2016). doi:10.1016/j.ijadhadh.2016.03.001

29. N. Lang, M. J. Pereira, Y. Lee, I. Friehs, N. V. Vasilyev, E. N. Feins, K. Ablasser, E. D. O'Cearbhaill, C. Xu, A. Fabozzo, R. Padera, S. Wasserman, F. Freudenthal, L. S. Ferreira, R. Langer, J. M. Karp, P. J. del Nido, A blood-resistant surgical glue for minimally invasive repair of vessels and heart defects. *Sci. Transl. Med.* **6**, 218ra6 (2014). doi:10.1126/scitranslmed.3006557 Medline

30. P. K. Campbell, S. L. Bennett, A. Driscoll, A. S. Sawhney, "Evaluation of absorbable surgical sealants: In vitro testing" (Covidien, 2005); www.covidien.com/imageServer.aspx/doc179399.pdf?contentID=14109&contenttype=application/pdf.

31. H. J. Kong, D. Kaigler, K. Kim, D. J. Mooney, Controlling rigidity and degradation of alginate hydrogels via molecular weight distribution. *Biomacromolecules* **5**, 1720–1727 (2004). doi:10.1021/bm049879r Medline

32. S. Nemir, H. N. Hayenga, J. L. West, PEGDA hydrogels with patterned elasticity: Novel tools for the study of cell response to substrate rigidity. *Biotechnol. Bioeng.* **105**, 636–644 (2010). doi:10.1002/bit.22574 Medline

33. R. B. Qaqish, M. M. Amiji, Synthesis of a fluorescent chitosan derivative and its application for the study of chitosan–mucin interactions. *Carbohydr. Polym.* **38**, 99–107 (1999). doi:10.1016/S0144-8617(98)00109-X

34. J. Li, W. R. K. Illeperuma, Z. Suo, J. J. Vlassak, Hybrid hydrogels with extremely high stiffness and toughness. *ACS Macro Lett.* **3**, 520–523 (2014). doi:10.1021/mz5002355

35. R. S. Rivlin, A. G. Thomas, Rupture of rubber. I. Characteristic energy for tearing. *J. Polym. Sci.* **10**, 291–318 (1953).

36. J. Tang, J. Li, J. J. Vlassak, Z. Suo, Adhesion between highly stretchable materials. *Soft Matter* **12**, 1093–1099 (2016). doi:10.1039/C5SM02305J Medline

37. E. T. Roche, C. L. Hastings, S. A. Lewin, D. E. Shvartsman, Y. Brudno, N. V. Vasilyev, F. J. O'Brien, C. J. Walsh, G. P. Duffy, D. J. Mooney, Comparison of biomaterial delivery vehicles for improving acute retention of stem cells in the infarcted heart. *Biomaterials* **35**, 6850–6858 (2014). doi:10.1016/j.biomaterials.2014.04.114 Medline

38. E. T. Roche, M. A. Horvath, I. Wamala, A. Alazmani, S.-E. Song, W. Whyte, Z. Machaidze, C. J. Payne, J. C. Weaver, G. Fishbein, J. Kuebler, N. V. Vasilyev, D. J. Mooney, F. A. Pigula, C. J. Walsh, Soft robotic sleeve supports heart function. *Sci. Transl. Med.* **9**, eaaf3925 (2017). doi:10.1126/scitranslmed.aaf3925 Medline

39. C. E. Morgan, V. S. Prakash, J. M. Vercammen, T. Pritts, M. R. Kibbe, Development and validation of 4 different rat models of uncontrolled hemorrhage. *JAMA Surg.* **150**, 316–324 (2015). doi:10.1001/jamasurg.2014.1685 Medline

40. A. K. Gaharwar, R. K. Avery, A. Assmann, A. Paul, G. H. McKinley, A. Khademhosseini, B. D. Olsen, Shear-thinning nanocomposite hydrogels for the treatment of hemorrhage. *ACS Nano* **8**, 9833–9842 (2014). doi:10.1021/nn503719n Medline

41. Q. Lin, D. Gourdon, C. Sun, N. Holten-Andersen, T. H. Anderson, J. H. Waite, J. N. Israelachvili, Adhesion mechanisms of the mussel foot proteins mfp-1 and mfp-3. *Proc. Natl. Acad. Sci. U.S.A.* **104**, 3782–3786 (2007). doi:10.1073/pnas.0607852104 Medline

42. M. Guvendiren, P. B. Messersmith, K. R. Shull, Self-assembly and adhesion of DOPA-modified methacrylic triblock hydrogels. *Biomacromolecules* **9**, 122–128 (2008). doi:10.1021/bm700886b Medline

43. B. K. Ahn, S. Das, R. Linstadt, Y. Kaufman, N. R. Martinez-Rodriguez, R. Mirshafian, E. Kesselman, Y. Talmon, B. H. Lipshutz, J. N. Israelachvili, J. H. Waite, High-performance mussel-inspired adhesives of reduced complexity. *Nat. Commun.* **6**, 8663 (2015). doi:10.1038/ncomms9663 Medline

44. H. K. Kjaergard, J. L. Velada, T. Pulawska, V. S. Ellensen, S. S. Larsen, D. A. Hollingsbee, Development of a model for measurement of adhesion strength of fibrin sealant to human tissue. *Eur. Surg. Res.* **31**, 491–496 (1999). doi:10.1159/000008729 Medline

45. K. Bundy, U. Schlegel, B. Rahn, V. Geret, S. Perren, An improved peel test method for measurement of adhesion to biomaterials. *J. Mater. Sci. Mater. Med.* **11**, 517–521 (2000). doi:10.1023/A:1008965926086 Medline

46. B. R. M. Perrin, M. Dupeux, P. Tozzi, D. Delay, P. Gersbach, L. K. von Segesser, Surgical glues: Are they really adhesive? *Eur. J. Cardiothorac. Surg.* **36**, 967–972 (2009). doi:10.1016/j.ejcts.2009.06.026 Medline

47. L. Li, M. Tirrell, G. A. Korba, A. V. Pocius, Surface energy and adhesion studies on acrylic pressure sensitive adhesives. *J. Adhes.* **76**, 307–334 (2001). doi:10.1080/00218460108030724

48. M. Pharr, J.-Y. Sun, Z. Suo, Rupture of a highly stretchable acrylic dielectric elastomer. *J. Appl. Phys.* **111**, 104114 (2012). doi:10.1063/1.4721777

49. B. Zhang Newby, M. K. Chaudhury, Effect of interfacial slippage on viscoelastic adhesion. *Langmuir* **13**, 1805–1809 (1997). doi:10.1021/la960962c